ACS APPLIED MATERIALS & INTERFACES

Research Article

www.acsami.org

Proton-Induced Trap States, Injection and Recombination Dynamics in Water-Splitting Dye-Sensitized Photoelectrochemical Cells

Nicholas S. McCool,[†] John R. Swierk,[‖] Coleen T. Nemes,[‖] Timothy P. Saunders,[†,⊥] Charles A. Schmuttenmaer,*[,‖] and Thomas E. Mallouk*[,†,‡,§]

[†]Department of Chemistry, [‡]Department of Biochemistry and Molecular Biology, and [§]Department of Physics, The Pennsylvania State University, University Park, Pennsylvania 16802, United States

[‖]Department of Chemistry and Engineering Sciences Institute, Yale University, 225 Prospect Street, P.O. Box 208107, New Haven, Connecticut 06520-8107, United States

Supporting Information

ABSTRACT: Water-splitting dye-sensitized photoelectrochemical cells (WS-DSPECs) utilize a sensitized metal oxide and a water oxidation catalyst in order to generate hydrogen and oxygen from water. Although the Faradaic efficiency of water splitting is close to unity, the recombination of photogenerated electrons with oxidized dye molecules causes the quantum efficiency of these devices to be low. It is therefore important to understand recombination mechanisms in order to develop strategies to minimize them. In this paper, we discuss the role of proton intercalation in the formation of recombination centers. Proton intercalation forms nonmobile surface trap states that persist on time scales that are orders of magnitude longer than the electron lifetime in TiO_2. As a result of electron trapping, recombination with surface-bound oxidized dye molecules occurs. We report a method for effectively removing the surface trap states by mildly heating the electrodes under vacuum, which appears to primarily improve the injection kinetics without affecting bulk trapping dynamics, further stressing the importance of proton control in WS-DSPECs.

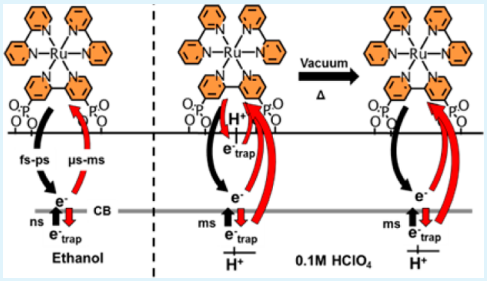

KEYWORDS: *water-splitting, solar energy, trap states, charge recombination, terahertz spectroscopy*

INTRODUCTION

Wide band gap semiconductors are ubiquitous in the field of solar photochemistry, finding use in a variety of applications such as dye-sensitized solar cells, photocatalysts for environmental remediation or fuel generation, and gas sensors. Of these semiconductors, titanium dioxide (TiO_2) has found the broadest range of application.[1] Unlike many metal oxides, TiO_2 is stable in both acidic and basic media, absorbs near-visible UV to generate a charge-separated state, has a high density of states in the conduction band and is a good photoconductor. There is also increasing interest in TiO_2 as an electronic material given that it is the most common support in dye-sensitized solar cells, and shows promise as a conductive protective layer for photocathodes.[2−5] As a result of the prevalence of TiO_2 in these applications, understanding electron transport in this material is extremely important.

Electron mobility in high surface area polycrystalline TiO_2 films is several orders of magnitude lower than in single-crystal TiO_2 due to an exponential distribution of trap states at energies below the conduction band edge.[6−9] In these films, the trap states are largely associated with particle−particle grain boundaries and oxygen vacancies.[9] Diffusion of electrons through these films is further limited by local electric field screening within the film by electrolyte in solution[7] as well as by a simple geometric restriction imposed by the porous nature of the film, as has been shown in porous Si films.[10] This forces the electron motion to be largely diffusion-based, i.e., a random walk through the film in order to exit the electrode at the back contact. Therefore, the electron collection efficiency relies on a complex diffusion pathway in the film composed of many trapping/detrapping events on the one to tens of nanoseconds time scale.[6,11,12]

Proton intercalation has been shown to widely occur in TiO_2 electrodes.[12−21] It can occur as a charge compensation mechanism for electron injection and has been shown to occur in solutions with very dilute proton concentrations ($-\log(a_{H^+}) = 23$).[16] Intercalation occurs by protons disrupting the lattice and forming stable Ti^{3+}—OH or Ti^{3+}—H bonds, which produce shallow traps near the conduction band (CB) edge of TiO_2.[17,20−23] Although the traps are shallow, the lifetime of a trapping event can be up to tens of milliseconds as a result of the electrostatic charge of the traps.[12] Because they are surface states, proton-induced trap states can contribute substantially to the rate of recombination with oxidized dyes on the surface.[24] Here, we use water-splitting dye-sensitized photoelectrochemical cells (WS-DSPECs) as a platform to

Received: May 5, 2016
Accepted: June 13, 2016
Published: June 13, 2016

© 2016 American Chemical Society

DOI: 10.1021/acsami.6b05362
ACS Appl. Mater. Interfaces 2016, 8, 16727−16735

further understand the trapping dynamics related to intercalated protons in TiO_2.

WS-DSPECs are an intriguing option for renewable solar fuel generation.[5] Modeled after the standard dye-sensitized solar cell (DSSC), a mesoporous metal oxide semiconductor anode (commonly TiO_2 or core−shell TiO_2/SnO_2[25,26]) is functionalized with a light absorbing molecular sensitizer and a water oxidation catalyst. Under illumination, an excited electron is transferred from the sensitizer into the semiconductor conduction band and oxidizing equivalents diffuse across the surface via a series of intermolecular electron transfers between dye molecules to create a spatially charge-separated state. The electron diffuses through the TiO_2 to a transparent conducting oxide and eventually through an external circuit to a dark cathode where protons are reduced to generate hydrogen while the reduced sensitizer on the surface is regenerated by electron transfer from the water oxidation catalyst.

In WS-DSPECs, regeneration of the dye relies on electrons from the water oxidation half reaction. Because this is a four-electron four-proton catalytic process, regeneration is relatively slow and, as a result, recombination of electrons from the TiO_2 with the oxidized dye molecules is the primary fate of photogenerated electrons, with as many as 98% of electrons rapidly recombining with dye molecules; less than 2% of injected electrons persist to time scales relevant to solar fuel production.[27]

Commonly in WS-DSPECs, the dye is deposited from an aqueous 0.1 M $HClO_4$ solution or from water as this produces a monolayer coating of dye with the most efficient hole transport kinetics.[28−31] However, we have previously demonstrated that depositing dye from protic solvents results in the formation of proton induced trap states that have a deleterious effect on overall device performance.[29] The mechanism by which the proton-induced trap states impacts overall device performance is poorly understood. Herein, we revisit the issue of proton intercalation in order to gain a more comprehensive understanding of why proton intercalation results in poor device performance.

By coupling transient absorption spectroscopy (TAS), which utilizes changes in dye absorbance to observe recombination kinetics, and time-resolved terahertz spectroscopy (TRTS), which probes mobile electrons once they are in the conduction band of the electrode, we are able to detail the fate of an electron from the time scale of injection (fs−ns) through the time scale of recombination (ns−ms). This enables a deeper analysis of the relationship between trapping events and recombination. We demonstrate that proton-induced trap states act as nonmobile acceptor states which promote charge recombination on the microsecond time scale. We also demonstrate that by applying a mild heat treatment under vacuum to samples freshly deposited with dye from $HClO_4$, the peak performance of these cells exceeds those prepared from aprotic solvents. This is likely a result of the vacuum treatment effectively removing the proton-induced trap states.[24]

EXPERIMENTAL SECTION

Photoanode Preparation. Bis(2,2′-bipyridine)(4,4′-diphosphonato-2,2′-bipyridine)-ruthenium bromide, [Ru(II)phos], was synthesized as previously reported.[32] Different TiO_2 pastes were used for different experiments. For THz spectroscopy, TiO_2 paste was synthesized as previously reported as this paste adhered well to the quartz substrates.[33] The paste used for all other experiments was synthesized via a modified procedure.[34] Briefly, 12 g of glacial acetic acid was added all at once to 58.6 g of rapidly stirring titanium isopropoxide (>97.0%, Sigma). The solution was stirred for 15 min and then added all at once to 290 mL of water. After stirring for 1 h, 4 mL of concentrated nitric acid was added and then the reaction was refluxed at 80 °C for 75 min. The reaction solution was distributed to bomb reactors and heated to 250 °C for 12 h. The resulting particles were sonicated using a horn (Branson, 450 W) to create a suspension and were then centrifuged and washed with ethanol three times. Following the third centrifugation, a solution of 6 g ethyl cellulose (Sigma, 48.0−49.5% w/w ethoxyl basis) in 56 g of terpineol (Sigma, 65% α-, 10% β-, 20% γ-mixture) and 300 mL of anhydrous ethanol were added to the particles and sonicated to resuspend the particles. The ethanol was then stripped via rotary evaporation to leave the final viscous and translucent TiO_2 paste. Photoanodes were prepared as previously reported using a doctor blading method[35] and then sintered at 300 °C for 20 min, 350 °C for 10 min and 500 °C for 30 min. Electrodes were sensitized with 100 μM Ru(II)phos in anhydrous, denatured ethanol or 0.1 M $HClO_4$ (aq) for 20 h to give identical surface coverages of 5×10^{-9} mol cm^{-2} μm^{-1}. Slides that received the vacuum-heating treatment were placed in a dark vacuum chamber under dynamic pumping using a standard oil pump at 200 mTorr with a trap to prevent backstreaming for 24 h at 80 °C (heating under vacuum ($HClO_4$−HV) treatment) following dye deposition.

Thicker films needed for THz measurements were made by doctor blading multiple times on a fused quartz substrate using one tape spacer each time with a curing step at 80 °C for 10 min between each deposition. The films were then sensitized and sealed using a 60 μm thick Surlyn (Solaronix) spacer and a second piece of quartz. The slides were hot-pressed together at 250 °C for 45 s to melt the Surlyn and seal the slides together. The empty space between the slides was vacuum-filled through a small hole in the top piece of quartz with 100 mM pH 6.8 potassium phosphate buffer that had been previously purged with N_2 to remove air. The samples were then sealed using a second piece of Surlyn and a microscope coverslip.

Measurements and Characterization. All photoelectrochemical experiments were carried out using a 300 W Xe arc lamp attenuated with an A.M. 1.5 filter to obtain an intensity of 100 mW/cm^2. A 410 nm long pass filter was placed in front of the sample to eliminate direct band gap excitation of the TiO_2. The photoanodes were tested in an H-cell configuration in 100 mM sodium phosphate buffer (NaPi) at pH 6.8. The anode and a Ag/AgCl (3 M NaCl) reference electrode were placed together in the anode compartment and a Pt mesh was placed in the cathode compartment, separated by a glass frit.

Chronoamperometry was measured using a Pine Instruments bipotentiostat. Prior to each experiment, the cathode compartment was purged with 5% hydrogen balanced with argon. The anode was then biased at 100 mV vs Ag/AgCl (3 M NaCl) and after several seconds was exposed to light for the duration of the experiment.

Chronopotentiometry was carried out using a Metrohm Autolab potentiostat operated in galvanostatic mode. The photoanode and Ag/AgCl (3 M NaCl) reference electrode were placed together in one compartment of an H-cell configuration and a Pt mesh acted as the counter electrode in the second compartment. Electrodes were held at open circuit conditions under illumination, and the generated open circuit photovoltage between the working and reference electrode was recorded.

For transient absorption spectroscopy (TAS) measurements, sensitized electrodes were placed in degassed 100 μM pH 6.8 KPi buffer and irradiated with 420 nm light through a monochromator. The samples were photoexcited with a 2 mJ 530 nm laser pulse.

The spectrometer used for time-resolved transient spectroscopy (TRTS) is described elsewhere.[36−40] Briefly, the output of a Spectra-Physics Ti:sapphire regenerative amplifier generating 35 fs pulses at 800 nm with a repetition rate of 1 kHz was split into 3 beams: a pump beam, a generation beam, and a detection beam. The pump beam was frequency-doubled to 400 nm then passed through a variable neutral density filter to a final power of 100 mW/cm^2. The generation beam was focused along with the second harmonic in air to generate a plasma which, in turn, generated the THz radiation used to probe the sample conductivity. The transmitted THz amplitude was detected

DOI: 10.1021/acsami.6b05362
ACS Appl. Mater. Interfaces 2016, 8, 16727−16735

using free-space electro-optic sampling with a ZnTe(110) crystal.[41] TRTS traces were fit with the following function:[42]

$$\Delta\mathrm{THz} = \left\{\Delta\mathrm{THz}_0 + \sum_{i=1}^{n} A_i\left[\exp\left(-\frac{t-t_0}{\tau_i}\right) - 1\right]\right\} \otimes \mathrm{G(fwhm)} \quad (1)$$

where THz_0 is a baseline offset, n is the number of exponentials used in the fit, t_0 refers to the excitation time-zero, A_i is the amplitude of the given component, and τ_i is the time constant associated with that component. G(fwhm) represents a normalized Gaussian instrument response function, and $\otimes$ is a convolution.

RESULTS

Photoelectrochemical Water Oxidation. Photoelectrochemical water oxidation requires a catalyst to drive the half reaction in these systems. Despite this, Fielden et al. recently reported photoelectrochemical water oxidation in a dye-sensitized cell without the intentional addition of a catalyst.[43] It is likely that this is a result of catalytically active metal impurities in the starting reagents or leached from glassware or apparati used in the experiments.[44,45] In this work, we observe the same effect, with oxygen evolution quantified in a well-established generator-collector electrode configuration[43,46−48] (Figure S1). The details of this experiment are discussed in the Supporting Information (SI). Because the identity of the water oxidation catalyst is not critical for this work, we used the active electrodes as prepared.

Recently, we analyzed the effect of the solvent from which the dye was deposited on the performance of WS-DSPECs.[29] Despite faster hole transfer across the surface between dye molecules, samples where dye was adsorbed from a 0.1 M $HClO_4$ aqueous solution had dramatically poorer performance than those prepared from neat ethanol. This was attributed to proton intercalation into the crystal lattice of the TiO_2, which resulted in long-lived, shallow trap states that hindered electron mobility. The effect of proton-induced trap states is visible in Figure 1a (red trace). In this case, the as-prepared electrodes from $HClO_4$ (Ru-$HClO_4$) show an initial current spike to 202 ± 29 $\mu A/cm^2$ before rapidly polarizing to below 5 $\mu A/cm^2$ after a few seconds. Interestingly, when Ru-$HClO_4$ slides are exposed to the HV treatment (Ru-$HClO_4$−HV, Figure 1a, blue), the peak performance of the devices recovers and reaches 772 ± 36 $\mu A/cm^2$. This is nearly double the peak photocurrent for as-prepared EtOH slides (Ru-EtOH, Figure 1a, black), which reaches an average peak photocurrent of 441 ± 19 $\mu A/cm^2$. However, the Ru-$HClO_4$−HV slides also appear to suffer from very rapid current polarization, similar to the Ru-$HClO_4$ slides.

In order to understand the differences in the polarization of these electrodes, samples were prepared using various combinations of soaking in $HClO_4$, depositing dye from EtOH, the HV treatment or additional sintering steps. Samples were prepared by soaking the electrodes in 0.1 M $HClO_4$ (aq) before (Figure 1b, red) and after (Figure 1b, black) dye deposition in order to determine if simply exposing the electrode to $HClO_4$ caused the poor performance. Samples were also prepared by subjecting electrodes soaked in $HClO_4$ to either the HV treatment (Figure 1b, pink) or a second sintering step (Figure 1b, green) before dye deposition to gain insight in to how effectively the HV treatment revitalizes the samples following exposure to $HClO_4$. The sintering temperature is expected to be high enough to anneal away any defects, while the HV treatment occurs at lower temperatures and might be expected to remove protons by a dehydration mechanism.

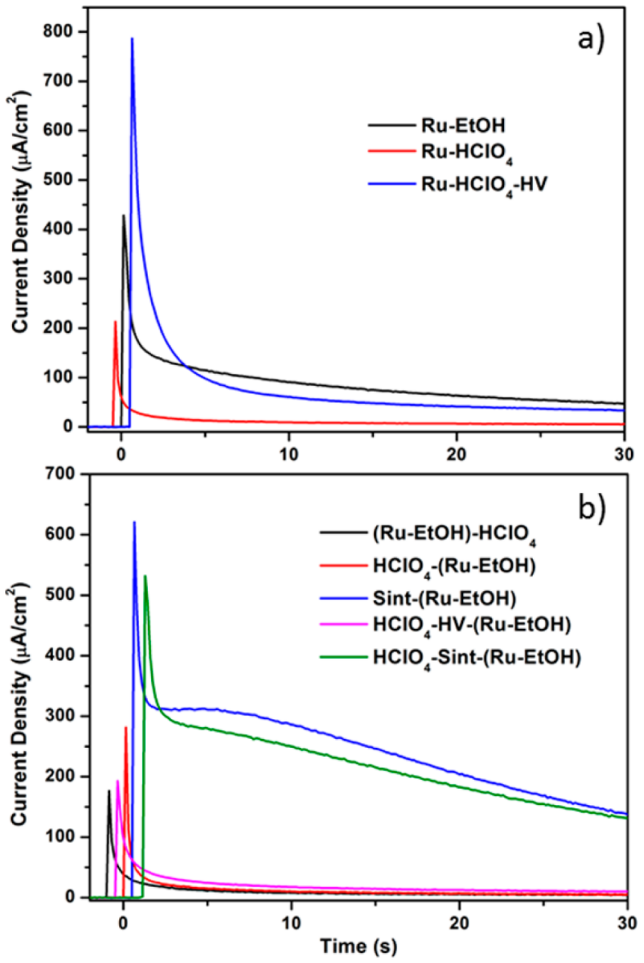

Figure 1. (a) Chronoamperometric water oxidation traces for TiO_2 electrodes in which Ru(II)phos was adsorbed from ethanol (black) and $HClO_4$ with (blue) and without (red) heated vacuum treatment prior to testing. (b) Chronoamperometric traces for TiO_2 electrodes sensitized with dye from EtOH with soaking steps in 0.1 M $HClO_4$(aq) after (black) and before (red) dye deposition, an $HClO_4$ soak and HV treatment (pink) or sintering step (green) before dye deposition, and an as-prepared TiO_2 slide sintered an additional time before dye deposition (blue). The dye deposition step is denoted with parentheses. Current was measured at a bias of 100 mV vs Ag/AgCl (3 M NaCl) in 100 mM pH 6.8 sodium phosphate buffer. Samples were illuminated from time zero for the duration of the experiment, traces are offset by 0.5 s from each other about time zero for clarity.

Additional samples were prepared by exposing fresh TiO_2 electrodes to a second sintering step (Figure 1b, blue) before dye deposition from EtOH in order to rule out any effects of the second sintering step on photoelectrochemical performance. The results are summarized in Figure 1b.

It is clear from the photocurrent data that any exposure to perchloric acid has a similar effect on the overall performance and polarization. Device performance is then only recovered if followed by the HV treatment, which improves the peak photocurrent, or a sintering step, which improves both the peak and extended performance. The HV treatment, when followed by the dye deposition step, still produces an electrode with poor performance and rapid polarization. This is in contrast with the electrodes that were subjected to an additional sintering step before dye deposition, which resulted in recovery of the initial photocurrent spike as well as slower polarization.

DOI: 10.1021/acsami.6b05362
ACS Appl. Mater. Interfaces 2016, 8, 16727−16735

Chronopotentiometry shows a similar trend in overall photovoltage. The photovoltage is defined as the difference between the potential of the Fermi level in the TiO_2 and the potential of the H_2O/O_2 couple (0.631 mV at pH 6.8).[29] Because the potential of the water/O_2 redox couple is fixed by pH, chronopotentiometry is a good probe of the quasi-Fermi energy of TiO_2 on longer time scales. Figure 2 shows the

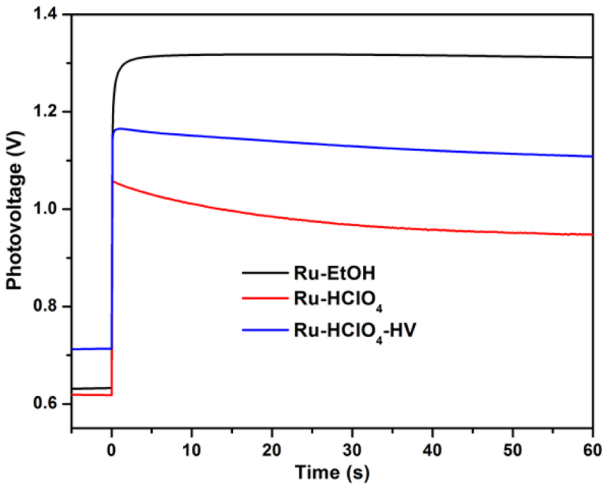

Figure 2. Representative chronopotentiometry traces for electrodes sensitized with Ru(II)phos dye from ethanol (black) and $HClO_4$ with (blue) or without (red) heated vacuum treatment. Electrodes held at open circuit galvanostatically in 100 mM pH 6.8 NaPi buffer and illuminated for the duration of the experiment beginning at time zero.

photovoltage generated by several different electrodes. Interestingly, the dark resting potential for these electrodes is about 600−700 mV negative of the H_2O/O_2 couple in the dark, meaning that the TiO_2 surface is not initially in electrochemical equilibrium with the H_2O/O_2 redox couple. This effect has been observed previously, and is connected with the fact that the TiO_2 surface is a poor catalyst for oxygen reduction in the dark.[27,29,49] This dark potential difference may be a consequence of electrons in long-lived trap states that are photogenerated before the photoelectrochemical experiment begins. As expected, upon illumination the open circuit photovoltage for Ru-EtOH electrodes grows smoothly over several seconds and reaches a value of about 1.3 V, which is stable for several minutes (Figure 2, black).

Similarly, upon illumination, the Ru-$HClO_4$ electrodes demonstrate the same instability in photovoltage as shown in the photocurrent (Figure 2, red). The photovoltage likely does not decay as quickly as the photocurrent because these are open circuit experiments and charge is not passing. Illumination results in a spike to nearly 1.1 V followed by a decay to below 1 V. In comparison, the Ru-$HClO_4$−HV electrodes both demonstrate a higher initial photovoltage than the Ru-$HClO_4$ electrodes as well as a more stable photovoltage (Figure 2, blue). Interestingly, however, these electrodes produce lower photovoltages than the Ru-EtOH slides despite having a higher initial photocurrent. A proposed mechanism for this unexpected result is detailed below.

Transient Absorption Spectroscopy. Protons are known to function as recombination centers in TiO_2.[12,24,29] Thus, in order to elucidate the mechanism by which protonation affects overall device performance, transient absorption spectroscopy (TAS) was used to measure recombination dynamics. When the dye injects an electron into the TiO_2, the formation of the oxidized dye leads to a bleach of the metal to ligand charge transfer (MLCT) band centered around 450 nm.[50] Following photoinjection, electrons from the TiO_2 then recombine with the oxidized sensitizer, which results in the recovery of the MLCT absorbance. By monitoring the bleaching and recovery of the MLCT absorbance the recombination kinetics can be directly measured. Charge injection typically occurs on the time scale of fs to ps,[51] which cannot be resolved with nanosecond transient absorption spectroscopy. However, by using an identical sensitizer and probing samples with comparable optical densities,[29] the magnitude of the bleach can yield information about the relative injection efficiencies resulting from different electrode treatments.

The recombination process in sensitized TiO_2 electrodes is complicated as a result of the exponential distribution of trap states below the CB[6−9] and is usually fitted using a stretched exponential function. A stretched exponential describes a single kinetic process that has a distribution of activation energies, e.g., recombination from various trap state energy levels. Figure 3

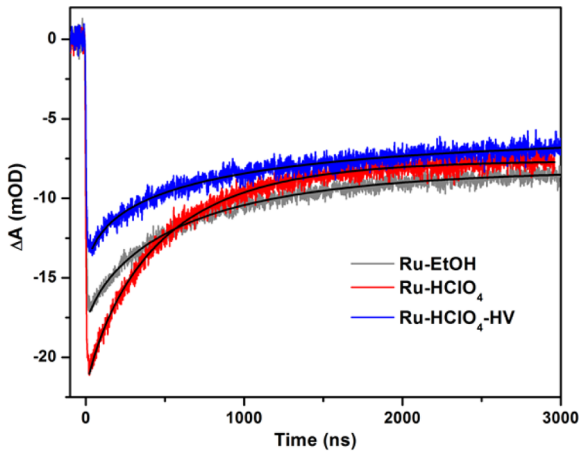

Figure 3. Transient absorption traces at 420 nm for TiO_2 electrodes sensitized with dye from ethanol (gray) and $HClO_4$ without (red) and with (blue) the heating vacuum treatment. Spectra were collected in N_2-purged 100 mM pH 6.8 potassium phosphate buffer. Stretched exponential fits are shown in black. Data were smoothed using a 3 point moving average.

shows the transients collected at 420 nm for Ru-EtOH, Ru-$HClO_4$, and Ru-$HClO_4$−HV through 3 μs while Figure S2 shows a representative transient for Ru-EtOH through 100 μs. Previously, we have demonstrated that these long-lived charges persist for tens of milliseconds.[27] Attempts to fit this long-lived recovery resulted in failure to reproduce the early kinetics of these TA traces and, as a result, the traces were only fit out to 100 μs. Because a majority of the recovery is observed in the first 3 μs, this window is shown in Figure 3. The transient absorption traces in Figure 3 were fitted with a stretched exponential of the form (Figure 3, black lines):

$$y = A \times \exp\left(\frac{-t}{\tau}\right)^{\beta} + y_0$$

where τ is the lifetime of the oxidized dye, β is a stretching parameter that represents the breadth of the distribution of activation energies for electron transfer, and can range from 0 to 1, A is a scaling factor, and y_0 is an offset. The average lifetime can be determined using the following analytical

DOI: 10.1021/acsami.6b05362
ACS Appl. Mater. Interfaces 2016, 8, 16727−16735

expression for the area under the stretched exponential curve:[52,53]

$$\left\langle \tau_{ww} \right\rangle = \frac{\tau}{\beta}\Gamma\left(\frac{1}{\beta}\right)$$

where Γ is the gamma function. A representative recombination rate, k_{rec}, can be taken as the reciprocal of $\langle\tau_{ww}\rangle$. Table S1 summarized the fitting parameters extracted from the stretched exponential fit.

Ru-EtOH (gray trace), Ru-$HClO_4$ (red trace), and Ru-$HClO_4$–HV samples (blue trace, Figure 3) all show a MLCT bleach characteristic for the formation of Ru(III). The injection efficiencies resulting from the three treatments are similar, with the Ru-$HClO_4$ having the highest injection yield and the Ru-$HClO_4$–HV having the lowest. The recombination kinetics for the Ru-$HClO_4$–HV samples (k_{rec} = 9.91 (±0.13) × 10^5 s^{-1}) are about twice as fast as for Ru-EtOH (k_{rec} = 4.76 (±0.20) × 10^5 s^{-1}), while recombination in Ru-$HClO_4$ is significantly more rapid (k_{rec} = 1.70 (±0.02) × 10^6 s^{-1}).

Time-Resolved THz Spectroscopy. The nature of protonation is directly related to trapping events in the TiO_2 which should ideally be probed directly. Whereas TAS is sensitive to changes in dye absorption related to changes in oxidation state, TRTS is sensitive to mobile electrons in the TiO_2. Conductivity is proportional to the product of mobility and charge density. Therefore, by utilizing a single material (i.e., TiO_2), the mobility is constant and any differences are due to differences in charge densities, which are directly related to electron injection efficiencies. Mobile electrons in the TiO_2 absorb/reflect THz radiation, which results in a decrease in transmitted THz amplitude.

Figure 4 shows the TRTS scans for Ru-EtOH (gray), Ru-$HClO_4$ (red), and Ru-$HClO_4$–HV (blue) slides. Fit of eq 1 are overlaid on the respective traces in black and fitting parameters are summarized in Table S2 in the SI. The injection component for Ru-EtOH and Ru-$HClO_4$–HV are fit with a triexponential; the Ru-$HClO_4$–HV required a forth exponential to describe the trapping dynamics. Ru-$HClO_4$ injection is well described by a biexponential with a third exponential to fit the trapping. Injection occurs over approximately 1 ns, which is consistent with our previous results.[42] As can be seen, after 900 ps, the Ru-EtOH slides exhibit a larger attenuation of the THz amplitude than Ru-$HClO_4$, which corresponds to nearly twice the density of mobile electrons within the material after 1 ns. However, in the case of the Ru-$HClO_4$–HV, the THz attenuation that was initially lost during the $HClO_4$ deposition step is mostly recovered by mildly heating the electrode under vacuum, reaching a maximum attenuation very similar to the Ru-EtOH samples after 1 ns. Between 1 and 1.5 ns, both samples exposed to $HClO_4$ show rapid trapping dynamics, demonstrated by the recovery of the THz amplitude, while the Ru-EtOH samples show very little change in THz amplitude after the injection finishes.

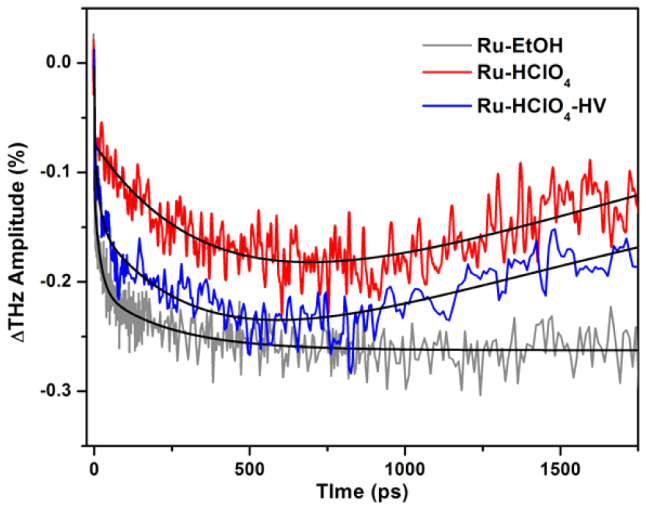

Figure 4. THz scans for quartz/TiO_2 slides sensitized with Ru(II)phos from ethanol (gray) and $HClO_4$, without (red) and with (blue) heating under vacuum after dye deposition. Spectra were collected in solvent-sealed devices using N_2 purged 100 mM pH 6.8 potassium phosphate buffer.

DISCUSSION

Interfacial Electron Transfer Dynamics. TAS and TRTS are complementary techniques; TAS probes the recombination of photoinjected electrons via the change in absorbance of the MLCT band of the dye, whereas TRTS can analyze the charge density directly in the material following charge injection. This allows for a broader understanding of the fate of electrons through the processes of injection, trapping, and eventually recombination.

The time scales of electron injection, recombination, and trapping under illumination are summarized in Scheme 1.

Injection from the sensitizer into the TiO_2 occurs on the fs to ns time scale,[51,54,55] with the electrons appearing in the conduction band on the ps to ns time scale.[42] The TRTS scans shown in Figure 4 agree with this picture, with mobile electrons

Scheme 1. Time Scales for the Electron Pathway from Charge Injection to Recombination, Favorable Electron Transfer Events Are Shown in Black, Unfavorable Are Shown in Red[a]

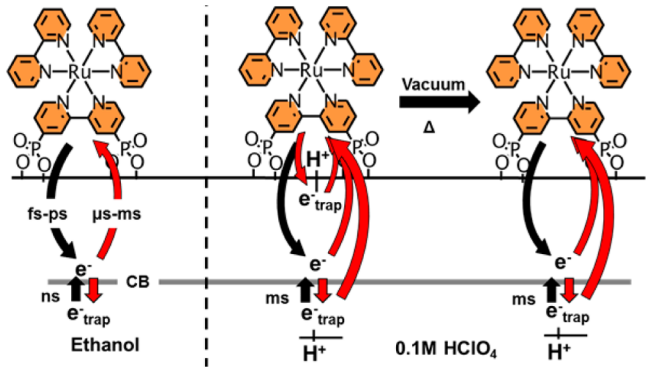

[a]Electrons are photoinjected into mobile conduction band (ethanol) or immobile proton induced surface trap states ($HClO_4$) on the fs–ns time scale. Recombination from the semiconductor occurs in the μs to ms range. In Ru-EtOH electrodes, trapped electrons persist for tens of nanoseconds before thermalizing and diffusing via a trapping/detrapping random walk process. Proton-induced trap states can be surface states that accept photoinjected electrons directly from the sensitizer or bulk states that can trap electrons from the conduction band. Proton-stabilized electrons remain trapped for tens of milliseconds and can readily recombine from surface states with oxidized dye molecules. Heating these electrodes under vacuum successfully removes surface states; however, bulk trap states remain unaffected.

DOI: 10.1021/acsami.6b05362
ACS Appl. Mater. Interfaces 2016, 8, 16727–16735

appearing on time scales of tens to hundreds of ps. Only mobile electrons in the CB of the TiO_2 absorb/reflect THz radiation so, as seen in Figure 4, the Ru-EtOH slides show a higher yield of mobile electrons when compared to the Ru-$HClO_4$ slides. In contrast, the TAS data (Figure 3) show that the Ru-EtOH slides have a weaker bleaching signal and, correspondingly, a lower injection yield than films sensitized from perchloric acid. This suggests that electrons are injected more efficiently in the case of the Ru-$HClO_4$, but that a greater fraction of them are injecting into nonmobile acceptor states. Injection into nonmobile surface states has been observed before in this system[42] and on ZnO sensitized with N719 dye.[56,57] The data in Figures 3 and 4 suggest that the "missing" photoinjected electrons in Ru-$HClO_4$ are in proton-stabilized trap states near the surface of the TiO_2. Electrons injected directly into or rapidly trapped by these nonmobile acceptor states are invisible to TRTS. This "missing" injection pathway is further supported by the fitting of the TRTS data. The Ru-EtOH samples are fit with a triexponential, with lifetimes of <0.5, 19.1, and 231.1 ps, whereas the injection process for Ru-$HClO_4$ samples only required a biexponential fit with lifetimes of 0.8 and 460.1 ps. At much longer time scales, trapping occurs in the Ru-$HClO_4$ electrodes and, in comparing the normalized scaling factor for injection and trapping (Table S2), it can be seen that with a lifetime of 2348 ps, all of the mobile electrons will be trapped by these proton-induced trap states. The Ru-EtOH slides show no trapping dynamics in the time scale of the experiments.

Recombination in Ru-$HClO_4$ samples is also more rapid, with the rate constant for recombination nearly 4 times larger than for Ru-EtOH. Qualitatively this can be seen by observing (Figure 3) that within 1 μs more than 50% of the injected electrons have recombined with the oxidized sensitizer in Ru-$HClO_4$, while at 3 μs only about 30% of the injected electrons in Ru-EtOH have recombined. The shorter lifetime observed in the Ru-$HClO_4$ samples can be explained by considering the nature of the proton-induced trap states. These trap states seem to dominate the trapping dynamics and are expected to be primarily surface states and electrostatically charged. As a result, the traps are energetically shallow (due to their charged nature) and can persist for up to tens of milliseconds,[12] or up 6 orders of magnitude longer than the average trapping lifetime in TiO_2 (one to tens of nanoseconds) and at best a similar time scale to recombination (100s of nanoseconds to milliseconds). Because these trap states are surface bound and long-lived, they have a large impact on recombination kinetics, reducing the early time lifetime of the electrons by 25%. In WS-DSPECs, rapid recombination is arguably the most significant pathway for loss of efficiency, with 98% of injected electrons recombining with a dye cation in less than 1 ms.[27]

Interestingly, when the as-prepared $HClO_4$ slides are subsequently exposed to heating under vacuum, the resulting TRTS scans demonstrate a nearly complete recovery of the mobile electron density in the material, as shown in Figure 4. The lifetime for the injection processes for the Ru-$HClO_4$–HV slides are <0.5, 16.5, and 402.3 ps, very similar to the Ru-EtOH samples aside from the longest lifetime component. Because the longest lifetime injection (positive) component for the Ru-$HClO_4$–HV samples is similar to that for the Ru-$HClO_4$ samples, it seems that this injection pathway could be tied to the proton-induced trap states, which is slowing down how rapidly the mobile electrons appear in the TRTS traces compared to the Ru-EtOH samples. When coupled to the TAS traces, which show a reduced injection efficiency for the Ru-$HClO_4$–HV slides when compared to untreated slides, this further demonstrates that the proton-induced trap states are acting as nonmobile acceptor states to charge injection.

While HV-treated slides show a higher density of mobile electrons than the untreated slides, electron trapping appears to remain an issue in Ru-$HClO_4$–HV samples. Surprisingly, it appears that all of the mobile electrons are being trapped in the Ru-$HClO_4$–HV samples as well, with a trapping lifetime of 1960.6 ps. Interestingly, this suggests that, despite effectively removing the trapping acceptor states, the HV treatment is not completely removing the trap states associated with proton intercalation. It is possible then that the HV treatment is merely removing proton-induced trap states on the surface of the TiO_2 and once electrons move from the surface, they are still trapped by inner proton-induced states.

The trapping found in Ru-$HClO_4$–HV electrodes is consistent with the intermediate recombination dynamics observed for Ru-$HClO_4$–HV samples in Figure 3. Figure 3 shows that the recombination kinetics for the Ru-$HClO_4$–HV samples are only half as fast as those of the original Ru-$HClO_4$ samples. Taken together, these results suggest that heating under vacuum successfully removes the acceptor states induced by proton intercalation into TiO_2; however an issue still remains at longer time scales.

Implications for WS-DSPEC Performance. In WS-DSPECs, the photovoltage and the corresponding device performance are controlled by the position of the Fermi level within the TiO_2, which in turn is dictated by the interplay of injection, recombination, and regeneration. We previously demonstrated that devices sensitized from ethanol had stable open-circuit photovoltages in excess of 1.1 V,[35] which is consistent with the results shown in Figure 2. We also see a peak current density in Ru-EtOH samples consistent with our previous results. Similarly, the Ru-$HClO_4$ slides behave consistently with expectations from earlier work.[29] Upon illumination, the Ru-$HClO_4$ electrodes show a spike in both the photocurrent as well as the photovoltage. The lower overall photovoltage generated from the Ru-$HClO_4$ electrodes indicates a lower Fermi energy in the TiO_2 as a result of proton-induced trap states, as was suggested by the faster recombination and trapping kinetics of Ru-$HClO_4$. This is consistent with shallow proton-induced trap states that promote recombination with oxidized dye molecules on the surface. This also suggests an explanation for the rapid decay in photovoltage as electrons are quickly trapped, and thus the mobile electron density within the material is reduced.

Following the HV treatment, the Ru-$HClO_4$–HV electrodes appear to initially recover in both photocurrent and photovoltage, which suggests that heating under vacuum has briefly eliminated the proton-induced trap states by removing the protons from the TiO_2. This has been previously demonstrated by Schulberg et al., who found that (Ba,Sr)TiO_3 that was initially intercalated with deuterium by annealing under a partial D_2 atmosphere could successfully be stripped of D through mild heating under vacuum or at elevated temperatures under an oxygen atmosphere.[24] The initial spike in photocurrent, which exceeds that of Ru-EtOH electrodes, is likely a result of more rapid hole transport kinetics across the surface, as previously measured for Ru-$HClO_4$ electrodes.[29] Interestingly, however, the photovoltage of Ru-$HClO_4$–HV does not exceed that of Ru-EtOH electrodes. This is likely a result of the poor stability of the Ru-$HClO_4$–HV electrodes, probably as result of bulk trap sites unaffected by the HV treatment. It is clear from

DOI: 10.1021/acsami.6b05362
ACS Appl. Mater. Interfaces 2016, 8, 16727–16735

Figure 4 that the recovery in performance from the HV treatment is temporary, where trapping still occurs at time scales faster than the EtOH. These electrodes polarize within the first 5 s of illumination (Figure 1) and, in fact, produce less photocurrent than the Ru-EtOH electrodes after only a few seconds. Previously, we have shown that degraded electrodes have similar impedance spectra as electrodes freshly prepared from perchloric acid, suggesting that protons generated by water oxidation at the surface of the electrode are intercalated.[29] This suggests that higher photocurrents, i.e., a higher flux of photoelectrochemically generated protons, would result in more rapid polarization in the photocurrent.

In order to gain a deeper understanding of the polarization of the Ru-$HClO_4$ and Ru-$HClO_4$–HV electrodes, samples were prepared with varying orders of exposure to perchloric acid as well as the HV treatment or an additional sintering step. The most obvious trend shown in Figure 1b is that any exposure to $HClO_4$ that is not immediately followed by sintering has a detrimental effect on device performance and stability. Because sintering the electrodes after exposure to the protic solvent not only recovers the initial peak performance but also slows the polarization, this suggests that it could be related to a structural effect. In fact, Mao et al. have demonstrated that, beginning with polycrystalline anatase nanocrystals, proton intercalation results in a dramatically disordered crystal lattice at the surface of the particle, while maintaining an ordered core.[22,23] They suggest that the intercalated protons act to stabilize the distorted lattice by binding to dangling bonds at the surface of the particle.

The instability of electrodes that were not exposed to the second sintering step suggests that something qualitatively similar could be happening with these devices during a soak in a protic solvent. This can also help explain why the electrode that was exposed to $HClO_4$, the HV treatment and then had dye deposited from EtOH performed similarly to the Ru-$HClO_4$ samples; the HV treatment appears to only remove the proton-induced trap states without restoring crystallinity to the TiO_2 film. Surface protons are possibly being driven off as water molecules, removing surface oxygen atoms along with the intercalated proton and leaving a further disrupted lattice as a result. A similar process has been observed with proton-exchanged layered titanates. Upon heating, water is lost to collapse the interlayer galleries resulting in materials with varying degrees of crystallinity.[58−60] As these topochemical dehydration processes are often reversible, reintercalation of protons may occur after HV treatment, explaining the bulk instability of HV electrodes. Water electrolysis increases the proton concentration at the surface of the electrode and may allow intercalation to occur as a charge compensation mechanism for photoinjected electrons.[61] It is also possible that the HV treatment fails to remove protons that migrate further in to the bulk. This hypothesis is consistent with the trapping dynamics observed in Figure 4; the HV treatment eliminates the trapping acceptor states on the surface without affecting the long term trapping dynamics because proton-induced traps persist in the bulk of the material.

CONCLUSIONS

Recombination of trapped electrons with oxidized dye molecules accounts for the fate of the vast majority of injected electrons in WS-DSPECs. Proton intercalation during exposure to protic solvents results in shallow, long-lived electrostatically charged trap states. These trap states act as nonmobile acceptors and trap electrons directly after injection. These trap states persist for much longer times than the typical lifetime of electrons in TiO_2, which results in efficient electron recombination with surface-bound oxidized dye molecules. As a result, proton-induced trap states exacerbate a problem that already dramatically lowers the efficiency of water splitting in dye-sensitized photoelectrochemical cells. These proton-induced trap states appear to be temporarily removed by heating under vacuum but are removed more completely by sintering the electrode after exposure to protic solvents. The weakness of the HV treatment suggests there might be various stages of proton intercalation, having both surface and bulk sites. This study should aid in the development of methods to address proton control in these devices and materials.

ASSOCIATED CONTENT

Supporting Information

The Supporting Information is available free of charge on the ACS Publications website at DOI: 10.1021/acsami.6b05362.

A detailed description of Clark-type experiment and oxygen detection measurements. Fitting parameters for TRTS traces in Figure 4 (PDF)

AUTHOR INFORMATION

Corresponding Authors

*E-mail: charles.schmuttenmaer@yale.edu (C.A.S.).
*E-mail: tem5@psu.edu (T.E.M.).

Present Address

⊥T.P.S.: Department of Chemistry, University of Wisconsin-Madison, Madison, WI 53706, U.S.A.

Notes

The authors declare no competing financial interest.

ACKNOWLEDGMENTS

This work was supported by the Office of Basic Energy Sciences, Division of Chemical Sciences, Geosciences, and Energy Biosciences, Department of Energy, under Contracts DE-FG02-07ER15911 and DE-FG02-07ER15909. N.S.M. thanks the National Science Foundation for support as a graduate fellow under Grant DGE1255832.

REFERENCES

(1) Diebold, U. The Surface Science of Titanium Dioxide. *Surf. Sci. Rep.* **2003**, *48* (5−8), 53−229.
(2) Fujishima, A.; Zhang, X.; Tryk, D. TiO_2 Photocatalysis and Related Surface Phenomena. *Surf. Sci. Rep.* **2008**, *63* (12), 515−582.
(3) Nakata, K.; Fujishima, A. TiO_2 Photocatalysis: Design and Applications. *J. Photochem. Photobiol., C* **2012**, *13* (3), 169−189.
(4) O'Regan, B.; Grätzel, M. A Low-Cost, High-Efficiency Solar Cell Based on Dye-Sensitized Colloidal TiO_2 Films. *Nature* **1991**, *353* (6346), 737−740.
(5) Swierk, J. R.; Mallouk, T. E. Design and Development of Photoanodes for Water-Splitting Dye-Sensitized Photoelectrochemical Cells. *Chem. Soc. Rev.* **2013**, *42* (6), 2357−2387.
(6) van de Lagemaat, J.; Frank, A. J. Nonthermalized Electron Transport in Dye-Sensitized Nanocrystalline TiO_2 Films: Transient Photocurrent and Random-Walk Modeling Studies. *J. Phys. Chem. B* **2001**, *105* (45), 11194−11205.
(7) Hendry, E.; Koeberg, M.; O'Regan, B.; Bonn, M. Local Field Effects on Electron Transport in Nanostructured TiO_2 Revealed by Terahertz Spectroscopy. *Nano Lett.* **2006**, *6* (4), 755−759.

DOI: 10.1021/acsami.6b05362
ACS Appl. Mater. Interfaces 2016, 8, 16727−16735

(8) Kopidakis, N.; Schiff, E. A.; Park, N.-G.; van de Lagemaat, J.; Frank, A. J. Ambipolar Diffusion of Photocarriers in Electrolyte-Filled, Nanoporous TiO_2. *J. Phys. Chem. B* **2000**, *104* (16), 3930−3936.
(9) van de Lagemaat, J.; Frank, A. J. Effect of the Surface-State Distribution on Electron Transport in Dye-Sensitized TiO_2 Solar Cells: Nonlinear Electron-Transport Kinetics. *J. Phys. Chem. B* **2000**, *104* (18), 4292−4294.
(10) Rao, P.; Schiff, E. A.; Tsybeskov, L.; Fauchet, P. M. Electron Time-of-Flight Measurements in Porous Silicon. *MRS Online Proc. Libr.* **1996**, *452*, 613−618.
(11) Wang, Q.; Zhang, Z.; Zakeeruddin, S. M.; Gratzel, M. Enhancement of the Performance of Dye-Sensitized Solar Cell by Formation of Shallow Transport Levels under Visible Light Illumination. *J. Phys. Chem. C* **2008**, *112* (17), 7084−7092.
(12) Halverson, A. F.; Zhu, K.; Erslev, P. T.; Kim, J. Y.; Neale, N. R.; Frank, A. J. Perturbation of the Electron Transport Mechanism by Proton Intercalation in Nanoporous TiO_2 Films. *Nano Lett.* **2012**, *12* (4), 2112−2116.
(13) Savory, D. M.; McQuillan, A. J. IR Spectroscopic Behavior of Polaronic Trapped Electrons in TiO_2 under Aqueous Photocatalytic Conditions. *J. Phys. Chem. C* **2014**, *118* (25), 13680−13692.
(14) Kavan, L.; Tétreault, N.; Moehl, T.; Grätzel, M. Electrochemical Characterization of TiO_2 Blocking Layers for Dye-Sensitized Solar Cells. *J. Phys. Chem. C* **2014**, *118* (30), 16408−16418.
(15) Betz, G.; Tributsch, H.; Marchand, R. Hydrogen Insertion (Intercalation) and Light Induced Proton Exchange at TiO2 (B)-Electrodes. *J. Appl. Electrochem.* **1984**, *14* (3), 315−322.
(16) Lyon, L. A.; Hupp, J. T. Energetics of the Nanocrystalline Titanium Dioxide/Aqueous Solution Interface: Approximate Conduction Band Edge Variations between $H_0 = -10$ and $H_- = +26$. *J. Phys. Chem. B* **1999**, *103* (22), 4623−4628.
(17) Kılıç, C.; Zunger, A. N-Type Doping of Oxides by Hydrogen. *Appl. Phys. Lett.* **2002**, *81* (1), 73.
(18) Peacock, P. W.; Robertson, J. Behavior of Hydrogen in High Dielectric Constant Oxide Gate Insulators. *Appl. Phys. Lett.* **2003**, *83* (10), 2025.
(19) Van De Walle, C. G.; Neugebauer, J. Universal Alignment of Hydrogen Levels in Semiconductors, Insulators and Solutions. *Nature* **2003**, *423* (6940), 626−628.
(20) Koudriachova, M. V.; de Leeuw, S. W.; Harrison, N. M. First-Principles Study of H Intercalation in Rutile TiO_2. *Phys. Rev. B: Condens. Matter Mater. Phys.* **2004**, *70* (16), 165421.
(21) Chen, W. P.; Wang, Y.; Chan, H. L. W. Hydrogen: A Metastable Donor in TiO_2 Single Crystals. *Appl. Phys. Lett.* **2008**, *92* (11), 112907.
(22) Chen, X.; Liu, L.; Yu, P. Y.; Mao, S. S. Increasing Solar Absorption for Photocatalysis with Black Hydrogenated Titanium Dioxide Nanocrystals. *Science* **2011**, *331* (6018), 746−750.
(23) Chen, X.; Liu, L.; Liu, Z.; Marcus, M. A.; Wang, W.-C.; Oyler, N. a; Grass, M. E.; Mao, B.; Glans, P.-A.; Yu, P. Y.; Guo, J.; Mao, S. S. Properties of Disorder-Engineered Black Titanium Dioxide Nanoparticles through Hydrogenation. *Sci. Rep.* **2013**, *3*, 1510−1517.
(24) McIntyre, P. C.; Ahn, J.-H.; Becker, R. J.; Wang, R.-V.; Gilbert, S. R.; Mirkarimi, L. W.; Schulberg, M. T. Deuterium in $(Ba,Sr)TiO_3$ Thin Films: Kinetics and Mechanisms of Incorporation and Removal during Annealing. *J. Appl. Phys.* **2001**, *89* (11), 6378.
(25) Sherman, B. D.; Ashford, D. L.; Lapides, A. M.; Sheridan, M. V.; Wee, K. R.; Meyer, T. J. Light-Driven Water Splitting with a Molecular Electroassembly-Based Core/Shell Photoanode. *J. Phys. Chem. Lett.* **2015**, *6* (16), 3213−3217.
(26) Wee, K.-R.; Sherman, B. D.; Brennaman, M. K.; Sheridan, M. V.; Nayak, A.; Alibabaei, L.; Meyer, T. J. An Aqueous, Organic Dye Derivatized SnO_2/TiO_2 Core/shell Photoanode. *J. Mater. Chem. A* **2016**, *4* (8), 2969−2975.
(27) Swierk, J. R.; McCool, N. S.; Mallouk, T. E. Dynamics of Electron Recombination and Transport in Water-Splitting Dye-Sensitized Photoanodes. *J. Phys. Chem. C* **2015**, *119* (24), 13858−13867.
(28) Hanson, K.; Losego, M. D.; Kalanyan, B. B.; Ashford, D. L.; Parsons, G. N.; Meyer, T. J. Stabilization of $[Ru(bpy)_2(4,4'-(PO_3H_2)bpy)]2+$ on Mesoporous TiO_2 with Atomic Layer Deposition of Al_2O_3. *Chem. Mater.* **2013**, *25* (1), 3−5.
(29) Swierk, J. R.; McCool, N. S.; Saunders, T. P.; Barber, G. D.; Mallouk, T. E. Effects of Electron Trapping and Protonation on the Efficiency of Water-Splitting Dye-Sensitized Solar Cells. *J. Am. Chem. Soc.* **2014**, *136* (31), 10974−10982.
(30) Knauf, R. R.; Kalanyan, B.; Parsons, G. N.; Dempsey, J. L. Charge Recombination Dynamics in Sensitized SnO_2/TiO_2 Core/Shell Photoanodes. *J. Phys. Chem. C* **2015**, *119* (51), 28353−28360.
(31) Caramori, S.; Cristino, V.; Argazzi, R.; Meda, L.; Bignozzi, C. A. Photoelectrochemical Behavior of Sensitized TiO_2 Photoanodes in an Aqueous Environment: Application to Hydrogen Production. *Inorg. Chem.* **2010**, *49* (7), 3320−3328.
(32) Gillaizeau-Gauthier, I.; Odobel, F.; Alebbi, M.; Argazzi, R.; Costa, E.; Bignozzi, C. A.; Qu, P.; Meyer, G. J. Phosphonate-Based Bipyridine Dyes for Stable Photovoltaic Devices. *Inorg. Chem.* **2001**, *40* (23), 6073−6079.
(33) Ito, S.; Chen, P.; Comte, P.; Nazeeruddin, M. K.; Liska, P.; Péchy, P.; Grätzel, M. Fabrication of Screen-Printing Pastes from TiO_2 Powders for Dye-Sensitised Solar Cells. *Prog. Photovoltaics* **2007**, *15* (7), 603−612.
(34) Ito, S.; Murakami, T. N.; Comte, P.; Liska, P.; Grätzel, C.; Nazeeruddin, M. K.; Grätzel, M. Fabrication of Thin Film Dye Sensitized Solar Cells with Solar to Electric Power Conversion Efficiency over 10%. *Thin Solid Films* **2008**, *516* (14), 4613−4619.
(35) Swierk, J. R.; McCool, N. S.; Saunders, T. P.; Barber, G. D.; Strayer, M. E.; Vargas-Barbosa, N. M.; Mallouk, T. E. Photovoltage Effects of Sintered IrO2 Nanoparticle Catalysts in Water-Splitting Dye-Sensitized Photoelectrochemical Cells. *J. Phys. Chem. C* **2014**, *118* (30), 17046−17053.
(36) Beard, M. C.; Turner, G. M.; Schmuttenmaer, C. A. Transient Photoconductivity in GaAs as Measured by Time-Resolved Terahertz Spectroscopy. *Phys. Rev. B: Condens. Matter Mater. Phys.* **2000**, *62* (23), 15764−15777.
(37) Turner, G. M.; Beard, M. C.; Schmuttenmaer, C. A. Carrier Localization and Cooling in Dye-Sensitized Nanocrystalline Titanium Dioxide. *J. Phys. Chem. B* **2002**, *106* (45), 11716−11719.
(38) Baxter, J. B.; Schmuttenmaer, C. A. Conductivity of ZnO Nanowires, Nanoparticles, and Thin Films Using Time-Resolved Terahertz Spectroscopy. *J. Phys. Chem. B* **2006**, *110* (50), 25229−25239.
(39) Beard, M. C.; Turner, G. M.; Schmuttenmaer, C. A. Subpicosecond Carrier Dynamics in Low-Temperature Grown GaAs as Measured by Time-Resolved Terahertz Spectroscopy. *J. Appl. Phys.* **2001**, *90* (12), 5915−5923.
(40) Nemes, C. T.; Koenigsmann, C.; Schmuttenmaer, C. A. Functioning Photoelectrochemical Devices Studied with Time-Resolved Terahertz Spectroscopy. *J. Phys. Chem. Lett.* **2015**, *6* (16), 3257−3262.
(41) Wu, Q.; Zhang, X. C. Free-Space Electro-Optic Sampling of Terahertz Beams. *Appl. Phys. Lett.* **1995**, *67* (1995), 3523−3525.
(42) Swierk, J. R.; McCool, N. S.; Nemes, C. T.; Mallouk, T. E.; Schmuttenmaer, C. A. Ultrafast Electron Injection Dynamics of Photoanodes for Water-Splitting Dye-Sensitized Photoelectrochemical Cells. *J. Phys. Chem. C* **2016**, *120* (11), 5940−5948.
(43) Fielden, J.; Sumliner, J. M.; Han, N.; Geletii, Y. V.; Xiang, X.; Musaev, D. G.; Lian, T.; Hill, C. L. Water Splitting with Polyoxometalate-Treated Photoanodes: Enhancing Performance through Sensitizer Design. *Chem. Sci.* **2015**, *6* (10), 5531−5543.
(44) Roger, I.; Symes, M. D. Efficient Electrocatalytic Water Oxidation at Neutral and High pH by Adventitious Nickel at Nanomolar Concentrations. *J. Am. Chem. Soc.* **2015**, *137* (43), 13980−13988.
(45) Trotochaud, L.; Young, S. L.; Ranney, J. K.; Boettcher, S. W. Nickel-Iron Oxyhydroxide Oxygen-Evolution Electrocatalysts: The Role of Intentional and Incidental Iron Incorporation. *J. Am. Chem. Soc.* **2014**, *136* (18), 6744−6753.
(46) Youngblood, W. J.; Lee, S.-H. A.; Kobayashi, Y.; Hernandez-Pagan, E. A.; Hoertz, P. G.; Moore, T. A.; Moore, A. L.; Gust, D.;

DOI: 10.1021/acsami.6b05362
ACS Appl. Mater. Interfaces 2016, 8, 16727−16735

Mallouk, T. E. Photoassisted Overall Water Splitting in a Visible Light-Absorbing Dye-Sensitized Photoelectrochemical Cell. *J. Am. Chem. Soc.* **2009**, *131* (3), 926−927.
(47) Zhao, Y.; Swierk, J. R.; Megiatto, J. D.; Sherman, B.; Youngblood, W. J.; Qin, D.; Lentz, D. M.; Moore, A. L.; Moore, T. A.; Gust, D.; Mallouk, T. E. Improving the Efficiency of Water Splitting in Dye-Sensitized Solar Cells by Using a Biomimetic Electron Transfer Mediator. *Proc. Natl. Acad. Sci. U. S. A.* **2012**, *109* (39), 15612−15616.
(48) Swierk, J. R.; Méndez-Hernández, D. D.; McCool, N. S.; Liddell, P.; Terazono, Y.; Pahk, I.; Tomlin, J. J.; Oster, N. V.; Moore, T. A.; Moore, A. L.; Gust, D.; Mallouk, T. E. Metal-Free Organic Sensitizers for Use in Water-Splitting Dye-Sensitized Photoelectrochemical Cells. *Proc. Natl. Acad. Sci. U. S. A.* **2015**, *112* (6), 1681−1686.
(49) Du, C.; Zhang, M.; Jang, J.; Liu, Y.; Liu, G.; Wang, D. Observation and Alterations of Surface States on Hematite Photoelectrodes. *J. Phys. Chem. C* **2014**, *118*, 17054−17059.
(50) Hanson, K.; Brennaman, M. K.; Ito, A.; Luo, H.; Song, W.; Parker, K. A.; Ghosh, R.; Norris, M. R.; Glasson, C. R. K.; Concepcion, J. J.; Lopez, R.; Meyer, T. J. Structure−Property Relationships in Phosphonate-Derivatized, Ru II Polypyridyl Dyes on Metal Oxide Surfaces in an Aqueous Environment. *J. Phys. Chem. C* **2012**, *116* (28), 14837−14847.
(51) Giokas, P. G.; Miller, S. A.; Hanson, K.; Norris, M. R.; Glasson, C. R. K.; Concepcion, J. J.; Bettis, S. E.; Meyer, T. J.; Moran, A. M. Spectroscopy and Dynamics of Phosphonate-Derivatized Ruthenium Complexes on TiO_2. *J. Phys. Chem. C* **2013**, *117* (2), 812−824.
(52) Lindsey, C. P.; Patterson, G. D. Detailed Comparison of the Williams−Watts and Cole−Davidson Functions. *J. Chem. Phys.* **1980**, *73* (7), 3348.
(53) Abrahamsson, M.; Johansson, P. G.; Ardo, S.; Kopecky, A.; Galoppini, E.; Meyer, G. J. Decreased Interfacial Charge Recombination Rate Constants with N3-Type Sensitizers. *J. Phys. Chem. Lett.* **2010**, *1*, 1725−1728.
(54) Asbury, J. B.; Hao, E.; Wang, Y.; Ghosh, H. N.; Lian, T. Ultrafast Electron Transfer Dynamics from Molecular Adsorbates to Semiconductor Nanocrystalline Thin Films. *J. Phys. Chem. B* **2001**, *105* (20), 4545−4557.
(55) Asbury, J. B.; Wang, Y.-Q.; Hao, E.; Ghosh, H. N.; Lian, T. Evidences of Hot Excited State Electron Injection from Sensitizer Molecules to TiO_2 Nanocrystalline Thin Films. *Res. Chem. Intermed.* **2001**, *27* (4−5), 393−406.
(56) Furube, A.; Katoh, R.; Hara, K.; Murata, S.; Arakawa, H.; Tachiya, M. Ultrafast Stepwise Electron Injection from Photoexcited Ru-Complex into Nanocrystalline ZnO Film via Intermediates at the Surface. *J. Phys. Chem. B* **2003**, *107* (17), 4162−4166.
(57) Furube, A.; Katoh, R.; Yoshihara, T.; Hara, K.; Murata, S.; Arakawa, H.; Tachiya, M. Ultrafast Direct and Indirect Electron-Injection Processes in a Photoexcited Dye-Sensitized Nanocrystalline Zinc Oxide Film: The Importance of Exciplex Intermediates at the Surface. *J. Phys. Chem. B* **2004**, *108* (33), 12583−12592.
(58) Rebbah, H.; Hervieu, M.; Raveau, B. The $CsTi_2NbO_7$ Type Layer Oxides: Ion Exchange Properties. *Mater. Res. Bull.* **1981**, *16* (2), 149−157.
(59) Tournoux, M.; Marchand, R.; Brohan, L. Layered $K_2Ti_4O_9$ and the Open Metastable TiO_2(B) Structure. *Prog. Solid State Chem.* **1986**, *17* (1), 33−52.
(60) Yin, S.; Uchida, S.; Fujishiro, Y.; Aki, M.; Sato, T. Phase Transformation of Protonic Layered Tetratitanate under Solvothermal Conditions. *J. Mater. Chem.* **1999**, *9* (5), 1191−1195.
(61) Lemon, B. I.; Hupp, J. T. Photochemical Quartz Crystal Microbalance Study of the Nanocrystalline Titanium Dioxide Semiconductor Electrode/Water Interface: Simultaneous Photoaccumulation of Electrons and Protons. *J. Phys. Chem.* **1996**, *100* (35), 14578−14580.

DOI: 10.1021/acsami.6b05362
ACS Appl. Mater. Interfaces 2016, 8, 16727−16735